SIMPLIFYING MSD MODELING BY USING CONTINUING DAMAGE ASSUMPTION AND PARAMETRIC STUDY: THE ROLE OF RIVET SQUEEZE FORCE

Garcia A N*, Mello Jr. A W S*, Irving P E**
***Institute of Aeronautics and Space (IAE) - Brazil, **Cranfield University - UK**

Keywords: *MSD, Continuing Damage, Squeeze Force*

Abstract

In this paper, a probabilistic model that incorporates continuing damage assumption as a MSD modeling simplification is presented and its output is compared to other work from the literature. The model is used to demonstrate how MSD onset behaviour is prevented when high rivet squeeze force is employed.

1 Introduction

Multiple Site Damage (MSD) is characterized by the development of simultaneous fatigue cracks at multiple sites in the same structural element. Among all aeronautical structures prone to develop MSD, riveted lap-splice joints in the fuselage have been identified as being the most susceptible [1]. When MSD cracks are present, crack propagation time decreases rapidly and the residual strength of the structural element is degraded. To investigate this failure mode, in this work a complete MSD assessment based on Monte Carlo (MC) simulation has been conducted for a typical aircraft three-row unstiffened lap-splice joint configuration.

Previous workers have approached MSD by considering the probabilistic nature of its occurrence, and have employed Monte Carlo techniques to simulate the stochastic nature of fatigue crack initiation at fastener holes and /or subsequent crack propagation, and therefore calculate the distribution of lives to MSD onset, link-up and ultimate failure. A comprehensive literature review on how MSD has been approached by many authors is presented in Garcia [2]. Surprisingly, the continuing damage assumption [3], which constitutes a simplifying alternative to a damage accumulation technique, has not been reported in any of the previous MSD methodologies presented, but for the first time in Garcia [2].

2 MSD Assessment Approach

In this work the MSD modelling procedures are separated into three different stages: fatigue crack initiation, deterministic crack propagation and probabilistic crack growth up to failure. The lap joint analysed is the one presented in Fig. 1. The geometry selected is of a typical fuselage lap joint section. The material is Al2024-T3 Clad T-L and the material properties employed are σ_{UTS} = 448 MPa, σ_{YS} = 331 MPa and K_{1C} = 32 MPa m$^{1/2}$.

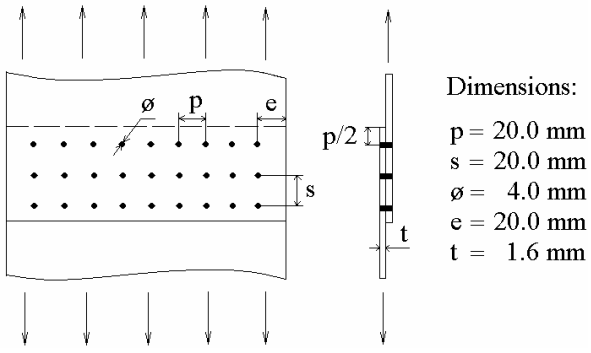

Fig. 1. Lap joint configuration analysed.

2.1 Fatigue Crack Initiation

To represent the fatigue crack initiation life 'N_0', a lognormal distribution of lives to achieve a crack size of 'a_0' is employed. Considering the external rows of a lap joint

(Fig.1), it is assumed that each pin-loaded hole has two fatigue critical locations (FCL) at 3 and 9 o'clock positions of the hole border. For each FCL, the normal distribution '$\log(N_0)$' is defined by the mean S-N fatigue life 'μ', the standard deviation 'σ' and the standard normal distribution 'α' given by,

$$\log(N_0) = \mu + \alpha.\sigma \qquad (1)$$

When a random value of 'α' is generated by Monte Carlo simulation, one initial damage scenario is created by attributing each FCL a different initial fatigue life given by eqn (1). The S-N fatigue curve properties used for the riveted holes is from Santgerma [4], and the values for 'μ[log]' and 'σ[log]', respectively, 5.6370 and 0.20 for an initial crack size a_o of 1.0 mm.

2.2 Deterministic Crack Propagation

Crack tips emanating from pin loaded fastener holes are subjected to mixed mode stress fields, and a Dual Boundary Element (DBE) program [5] calculates both K_I and K_{II} components. A mixed mode stress intensity range ΔK_{eff} was calculated using the Tanaka [6] expression,

$$\Delta K_{eff} = \sqrt{\Delta K_I^2 + 2\Delta K_{II}^2} \qquad (2)$$

The Paris equation is used to calculate the crack growth rate (da/dN), given as a function of the effective stress intensity factor (ΔK_{eff}),

$$\frac{da}{dN} = C(\Delta K_{eff})^m \qquad (3)$$

Material constants C and m values are C = 6.09E-11, and m = 2.6, obtained from Salgado [5]. Crack growth lives are then calculated in the usual way using eqn (3), with a starting crack length a_o of 1.0 mm, the initiation crack size. As cracks grow, the Swift [7] criterion is used to define link-up.

According to Swift [7], link-up of a lead crack and a MSD crack would occur when the intact ligament stress between them reaches the yield strength of the material (plane stress condition – thin sheets), i.e, when the two plastic zones ahead of the crack tip touch each other as schematically illustrated in Fig. 2.

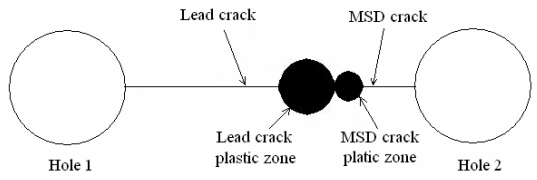

Fig. 2. Schematic of Swift link-up criterion for a lead and a MSD cracks.

The same intuitive link-up criterion, as proposed by Swift, has been investigated experimentally and via FE analysis but for the case of a crack approaching an undamaged hole, as schematically illustrated in Fig. 3, demonstrating good agreement [4].

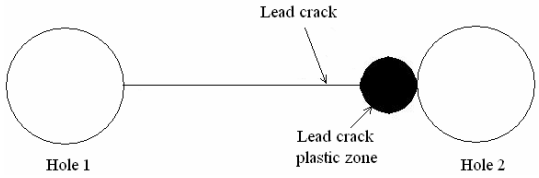

Fig. 3. Schematic of link-up criterion for a lead crack and an undamaged hole.

After link-up takes place, as illustrated in Fig. 2 and 3, continuing damage assumption [3] is employed in this work as illustrated in Fig. 4.

The continuing damage, as described by Gallagher [3], is intended to provide an orderly and progressive path for a crack that may cause structural failure, i.e, a crack size a_{cd} = 0.127 mm (0.005 in) is assumed to start from the opposite hole border to where link-up took place, as illustrated in Fig. 4. In his work, Gallagher refers to a 0.127 mm corner crack size. In this work, the continuing damage is performed by a through-the-thickness crack size a_{cd} = 0.127 mm.

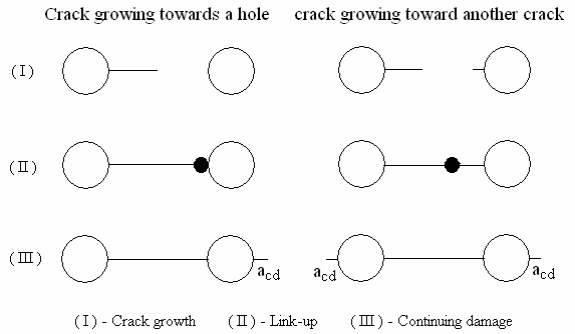

Fig. 4. Continuing damage assumption illustration.

All the MSD probabilistic models reported by Garcia [2] use a damage accumulation technique, opposed to continuing damage assumption from this work, to re-initiate crack growth after crack link-up has taken place, as sketched in Fig. 5.

From Fig. 5, it can be seen that a lead crack 'a_{lead}' starts to grow in (1) and it links-up in (2). Before or after link-up takes place, some possible situations for re-initiation of fatigue crack growth are illustrated in, respectively, (3) and (4). In models that use a damage accumulation technique, as a_{lead} grows (by adding pre-defined crack increment sizes 'Δa') the stress level a point 'a' changes at each different Δa value added; and consequently the initial fatigue life allocated for point 'a' has to be updated. In order to update the initial fatigue life at point 'a', Miner rule for damage accumulation calculation [8] is widely employed. If (2) is achieved, then (4) can occur where 'a_1' and 'a_3' enter the crack propagation model via Miner rule as well.

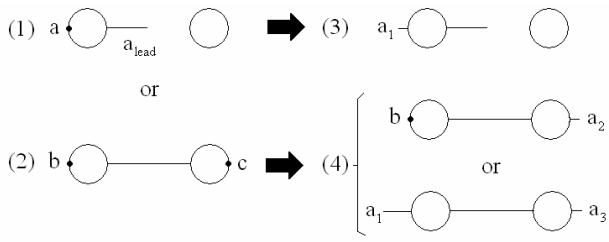

Fig. 5. Sketch of a damage accumulation technique for crack growth re-initiation.

In the case of multiple crack growth analysis via probabilistic MSD assessment models, the use of a damage accumulation technique, as illustrated in Fig. 5, increases considerably the analysis burden if the analyst has to stop at each crack increment size to consider changes in stress levels at undamaged fatigue critical locations (FCLs) such as points 'a', 'b' and 'c'. Therefore, the use of a damage accumulation technique for re-initiation of fatigue cracks can only justify itself in case it can be automatically taken into account by a step-routine incorporated into computer codes employed for crack growth analysis. In case a step-routine for continuing damage calculation cannot be incorporated, continuing damage assumption is a simplifying alternative; as it will be demonstrated in sections to come.

2.3 Probabilistic Crack Growth

In order to represent the probabilistic nature of the fatigue crack growth, the Xing [9] formulation will be used to expand the Monte Carlo simulation applied to numerical techniques, such as the DBEM. Taking the logarithm on both sides of eqn (3) it follows,

$$\log \frac{da}{dN} = \log C + m \log\left(\Delta K_{eff}\right) \qquad (4)$$

To represent the stochastic nature of crack propagation, a normally distributed variable $Z \sim N(0, \sigma_z^2)$ is added to the logarithm of the fatigue crack growth law in eqn (4),

$$\log \frac{da}{dN} = \log C + m \log\left(\Delta K_{eff}\right) + Z \qquad (5)$$

Considering the properties of the standard normal distribution, the probability that a measurement will fall in a range $Z \le Z_p$ is given by $P(Z \le Z_p) = p$, and Z_p can be written as,

$$Z_p = \alpha_p \sigma_z \qquad (6)$$

When the probability 'p' is given, α_p can be obtained from the standard normal distribution. For example, when $p = 50\%$, $\alpha_p = 0$, leading $Z_p = 0$ in eqn (6), therefore eqn (5) becomes the deterministic average fatigue crack growth rate represented by eqn (4). The probabilistic crack growth rate, represented by eqn (5), can be simplified if the value of 'm' is assumed as a mean constant value and the probabilistic character of crack growth is attributed to the constant 'C', assumed as a lognormal distribution. Therefore, eqn (5) and (6) can be re-arranged as,

$$\log\left(\frac{da}{dN}\right)_p = \log C_p + m\log\left(\Delta K_{eff}\right) \qquad (7)$$

Where $\log C_p = \log C + \alpha_p \sigma_z$ is now a random variable normally distributed with mean $\log C$ and variance σ_z^2. Eqn (7) can be re-written as,

$$\frac{da}{dN} = [C\exp(\alpha_p \sigma_z)](\Delta K_{eff})^m \qquad (8)$$

For a given value of α_p, the number of cycles N_f to grow a crack from an initial crack size 'a_0' up to a crack size 'a_f' is obtained from direct integration of eqn (8),

$$N_f = \frac{1}{C\exp(\alpha_p \sigma_z)} \int_{a_0}^{a_f} \frac{da}{(\Delta K_{eff})^m} \qquad (9)$$

Based on Virkler's [10] findings, it is assumed here that each initial damage scenario has a unique α_p value. In this work $\sigma_z[\log] = 0.043$ has been assumed, following Proppe [11].

3 Results

3.1 MSD Assessment Approach Comparison

Regarding the MSD methodology proposed in section 2, the MSD assessment model is employed for analysing the lap joint configuration, presented in Fig. 1, and the results compared to experimental work [12] and to other MSD models from the literature. The results from this work are presented in Fig. 6.

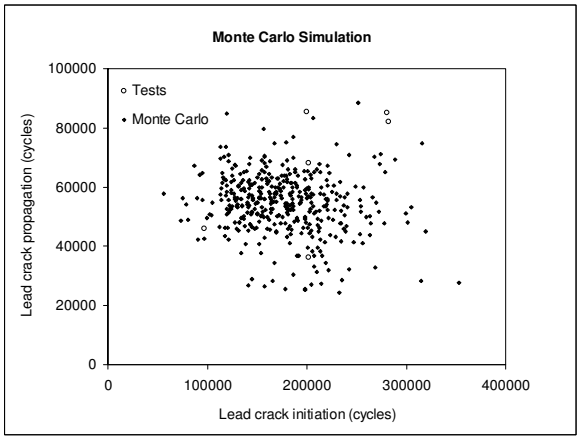

Fig. 6. Monte Carlo Simulation Comparison.

As found in other published simulations for MSD assessment, for instance Santgerma [4], Proppe [11], Kebir [13] and Cavallini [14], Fig. 6 shows that lives to failure are dominated by the crack initiation phase. It can be noted that for the Monte Carlo simulations the total initiation life varies from 55,758 to 352,684 cycles, whereas propagation lives are between 24,206 to 88,382 cycles.

Considering the 6 experimental test points from Fig. 6, the total initiation life varies from 97,000 to 281,950 cycles, whereas propagation lives are between 36,200 to 85,368 cycles and, therefore, the spread of predicted lives encloses the scatter of the experimental lives for both initiation and propagation stages. It can also be seen that the 6 experimental test points demonstrate a spread comparable to the 400 Monte Carlo simulations in both initiation and propagation axis. This observation is found in the majority of previous comparisons of Monte Carlo simulations to experimental MSD data from the literature (Fig. 7 to 10), despite of the geometry and loading conditions of the experimental data used for comparison.

In the case of Fig. 6, it is possible that were 400 experiments to be performed the observed scatter could be greater than the current simulations data set; but this issue can not be addressed here due to the small number of test points. As it can also be seen from Fig. 7 to 10, the number of experimental points employed for comparison is usually 5 to 6 tests.

What can be stated from Fig. 6 is that the simulations were able to enclose and, therefore, to represent the experimental test data used for comparison purposes, demonstrating its effectiveness.

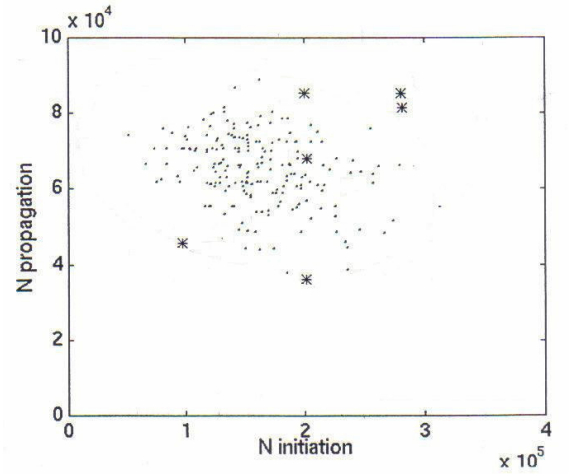

Fig. 7. MSD assessment from the literature and comparison to experimental work [4].

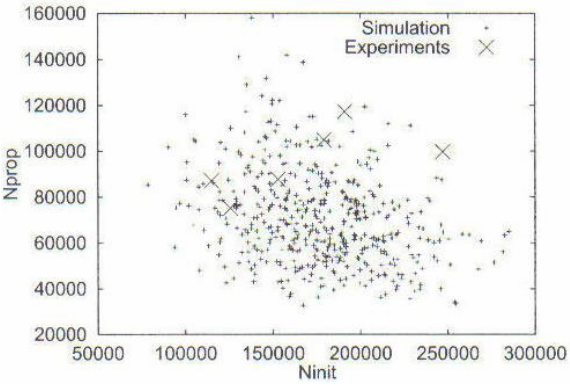

Fig. 8. MSD assessment from the literature and comparison to experimental work [11].

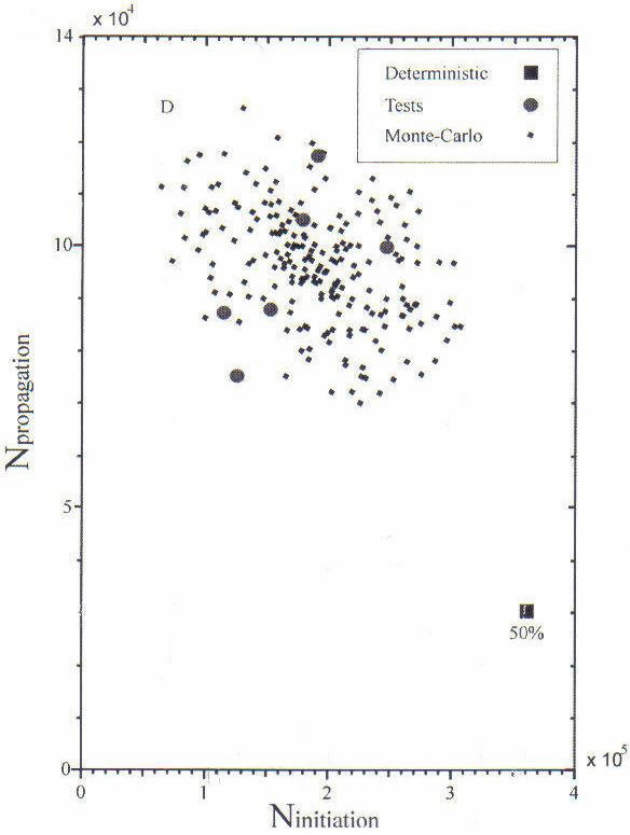

Fig. 9. MSD assessment from the literature and comparison to experimental work [13].

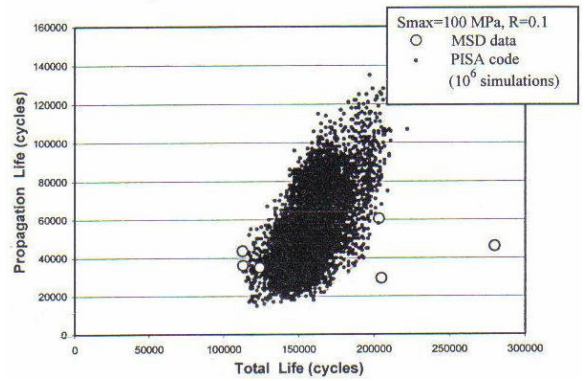

Fig. 10. MSD assessment from the literature and comparison to experimental work [14].

3.2 Parametric Study: The Hole of Rivet Squeeze Force

In order to evaluate the effect of rivet squeeze force on MSD progression, an experimental work was performed as described in Garcia [2]. The lap joint geometrical configuration tested is of a strap containing 3 rows of rivets and 1 rivet per row. Countersunk rivets (NAS1097AD5-5 of aluminium 2117) were used to attach the sheets mechanically and there was no bonding or sealant between the mating sheets; the assembly was dry. The lap joint sheet material is Al2024-T351 Clad L-T. The geometrical configurations from Fig. 11 are l = 250 mm, c = 40 mm, e = 10 mm, p = 20 mm, W = 20mm, t = 1.6 mm and d reamed to 4 mm.

The testing procedures consist of fatigue testing to failure the strap lap joint illustrated in Fig. 11 under two different stress levels (100 and 120 MPa), with constant amplitude loading ($R = S_{min}/S_{max} = 0.1$) and 20 Hz frequency; according to the test matrix presented in Table 1. As it can be seen from Table 1, three different rivet squeeze force values 'F_{sq}' were considered: 10, 16 and 24 KN which are respectively, low, mean and high rivet squeeze forces. For each testing configuration 21 samples were tested.

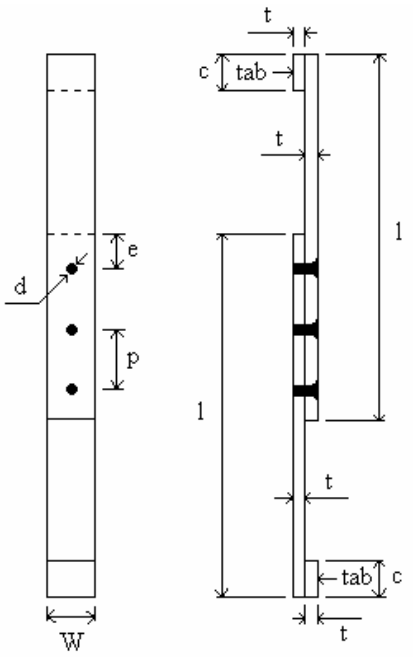

Fig. 11. Lap joint test specimen geometry.

Table 1. Testing matrix.

Test	Maximum Stress (MPa)	R	F_{sq} (KN)
1	100	0.1	10
2			16
3			24
4	120	0.1	10
5			16
6			24

The experimental work results are presented in Fig. 12. From Fig. 12 it can be seen the effect of rivet squeeze force on time to failure (cycles), also called time to crack initiation (TTCI), for the 6 testing configurations from Table 1. For both stress levels (100 and 120 MPa) the increase of squeeze force increases the TTCI at all range of cumulative probabilities, with the greater stress range producing the smallest lives. In the case of 100 MPa stress level and considering the 0.5 cumulative probabilities, for example, for squeeze forces varying from 10 to 16 KN, 16 to 24 KN and 10 to 24 KN the increase in TTCI is, respectively, by factors of 2.4, 2.9 and 6.9. While for the case of 120 MPa stress level, the increase in TTCI for squeeze forces varying from 10 to 16 KN, 16 to 24 KN and 10 to 24 KN are, respectively, by factors of 2.6, 1.9 and 5.0 for the same probability level.

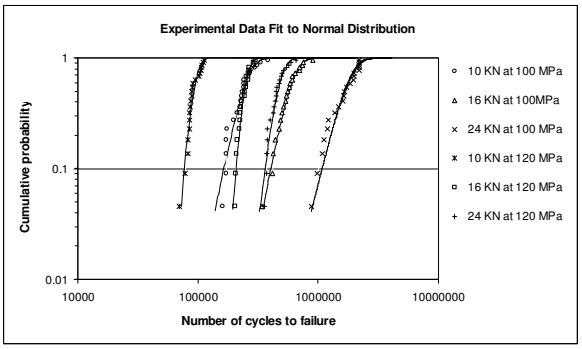

Fig. 12. Experimental work results.

To compare the effect of different rivet squeeze forces on MSD probabilistic behaviour, two cases from the test results presented on Fig. 12 are considered. These cases are of a mean and a high squeeze force values, respectively,

16 and 24 KN, at 100 MPa maximum stress level and R = 0.1. For each one of these cases 400 Monte Carlo simulations were performed, and the input values for the simulations, taken from the experimental results from Fig. 12, are presented in Table 3.

Table 3. Input for the Monte Carlo simulations considering different rivet squeeze force values.

F_{sq} (KN)	$\bar{x}$ (cycles)	s (cycles)	$\bar{x}$ log (cycles)	s log (cycles)
16	573,893	133,096	5.7478	0.1005
24	1,652,713	447,697	6.2014	0.1274

Notation: $\bar{x}$ is the mean time to crack initiation
s is the standard deviation

The results from the Monte Carlo simulations are presented in Fig. 13 and a resume of the average behaviour from these simulations is presented in Table 4.

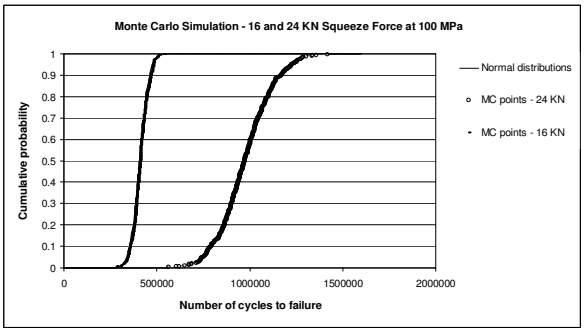

Fig. 13. Monte Carlo simulation results for input variables from Table 3.

Table 4. Monte Carlo simulation results using input values from Table 3.

Squeeze Force (KN)	$\overline{TTCI}$ (cycles)	$\overline{TCP}$ (cycles)	$\overline{N_f}$ (cycles)	MSD-like scenarios (%)
16	353,139	53,450	406,589	70.2
24	919,481	57,750	977,231	28.0

Notation:
$\overline{TTCI}$ is the mean time to crack initiation
$\overline{TCP}$ is the mean time for crack propagation
$\overline{N_f}$ is the mean time to failure ($\overline{TTCI} + \overline{TCP}$)

The results presented in Table 4 show that when the rivet squeeze force is increased from 16 to 24 KN, the $\overline{TTCI}$ is increased by a factor of 2.6, while the $\overline{TCP}$ is increased by a factor of 1.1; leading to an increase of the $\overline{N_f}$ by a factor of 2.4. These results show that the $\overline{TTCI}$ is far more sensible to changes in squeeze force values than the $\overline{TCP}$. It has also to be noted that the number of MSD-like scenarios (the number of simulations that developed at least two cracks) decrease with an increase of squeeze force. This result is consistent to the corresponding $\overline{TCP}$ values for the cases of 16 and 24 KN squeeze forces. Garcia [15] has demonstrated that an increase in the number of MSD-like scenarios decreases the $\overline{TCP}$ due to an increase in crack interaction effects, leading to smaller times for crack propagation.

From Fig. 13 it can be seen that the cumulative failure distribution inclination from the 'MC points – 16 KN' is smaller than the one from the 'MC points – 24 KN'. A decrease in inclination is related to a more severe MSD condition [2]. Small inclinations lead to a decrease in the range of number of cycles to failure; and once MSD starts, the probabilities of failure increase much faster in time (cycles) than for the case of large cumulative distribution inclinations. The increase in MSD severity can also be verified by the increase in MSD-like scenarios from Table 4 for the intermediate rivet squeeze force (16 KN).

The results from Fig. 3 and Table 4 show that high rivet squeeze force, beyond retarding the whole failure process, also lead to a decrease in MSD-like scenarios. The direct conclusion from these results is that high rivet squeeze force is extremely beneficial for MSD prevention since it helps to decrease the number of nucleated cracks in the same row of holes. Unfortunately the use of different squeeze force input values and its effect on MSD probabilistic failure behaviour has not been reported from the literature [2]; and no comparison to the results from this section can be done to other publication.

4 Summary

- The mean time to initiation of fatigue cracks, both in cycles and in log (cycles), increases when the squeeze force varies from a low to a high value, despite the stress level employed; and with the smallest stress range producing the biggest lives;
- Beyond improving the mean time for initiation of fatigue cracks, the high squeeze force test specimens provided the highest standard deviation (scatter) values, both in cycles and in log (cycles), despite of the stress level employed, and with the smallest stress range producing the biggest scatters;
- The MSD model provided good agreement with published experimental work on fatigue of lap splice joints where both crack initiation and propagation stages from the simulations were able to enclose the experimental data scatter; and the mean lives to crack initiation and propagation were similar to experimental data;
- The spread of the experimental data at both initiation and propagation lives was as large as that of the entire simulations; and this behaviour is also verified from other published work;
- By comparing the MSD model from this work to other published work, for the same lap joint geometrical configuration and loading conditions, it could be verified that continuing damage assumption (proposed in this work) can be used as a valid and simplifying option to a damage accumulation technique for fatigue crack re-initiation and growth;
- When MSD assessment was performed using the input parameters from the high squeeze force S-N data, compared to the same assessment but using the S-N data input from a mean squeeze force value, the results indicated that the whole MSD failure process was retarded and the number of MSD-like scenarios considerably reduced, demonstrating that high squeeze force is extremely beneficial for MSD prevention.

5 Acknowledgments

The authors would like to express their appreciation to Dr. Nelson Krahenbuhl Salgado (EMBRAER) for his help on the dual boundary element method technique, the Civil Aviation Authority (CAA) from the U.K. and the Brazilian Air Force (FAB) and for sponsoring this work.

References

[1] AAWG. Recommendations for Regulatory Action to Prevent Widespread Fatigue Damage in the Commercial Airplane Fleet. *A Report of the Airworthiness Assurance Working Group (AAWG) for the Aviation Rulemaking Advisory Committee Transport Aircraft and Engine Issues*, 1999.

[2] Garcia A N. *Multiple Site Damage of Aeronautical Riveted Joints*. Ph.D. Thesis, Cranfield University, UK, Sept. 2005.

[3] Gallagher, J. P., Giessier, F. J., Berens, A. P., *USAF damage tolerant design handbook: guidelines for the analysis and design of damage tolerant aircraft structures*, Flight Dynamics Laboratory, Wright-Patterson Air Force Base, Ohio, May 1984.

[4] Santgerma A. *Developpement d'Une Methodologie de Prevision du Comportement des Strutures d'Avions Civils en Presence de Dommages Multiples de Fatigue*. Doctorate Thesis, Department of Mechanical Engineering, Toulouse, 1997.

[5] Salgado N K. *Damage Tolerance Design System DTD Computer Code – V. 5.0*. Empresa Brasileira de Aeronautica, S. J. Campos – S. P., Brazil, 1999.

[6] Tanaka K. Fatigue Crack Propagation from a Crack Inclined to the Cyclic Tensile Axis. *Engineering Fracture Mechanics*, Vol. 6, pp. 493-507, 1974.

[7] Swift T. Damage Tolerance Capacity. *Fatigue of Aircraft Materials-Proceedings of the Specialists' Conference, Dedicated to the 65th Birthday of J. Schijve*, Delft University, pp. 351-387, 1992.

[8] Miner, M. A., Cumulative damage in fatigue, *Trans. ASME J. Appl. Mech.* No. 12, A159-A164, 1945.

[9] Xing J and Hong Y J. A Maximum Likelihood Method for Estimates of the Statistics of the Crack Growth Behaviour. *International Journal of Pressure Vessels and Piping,* Vol. 76, pp. 641-646, 1999.

[10] Virkler D A, Hillberry B M and Goal P K. The Statistical Nature of Fatigue Crack Propagation. *Journal of Engineering Materials and Technology*, Vol. 101, pp. 148-153, 1979.

[11] Proppe C. Probabilistic Analysis of Multi-Site Damage in Aircraft Fuselages. *Computational Mechanics*, Vol. 30, pp. 323-329, 2003.
[12] Foulquier J. *Fatigue Tests on Simple Lap Joint Specimens,* Report SMAAC TR-3.2-04-1.3/AS, 1997.
[13] Kebir A, Roelandt J M and Gaudin J. Monte-Carlo Simulations of Life Expectancy Using the Dual Boundary Element Method. *Engineering Fracture Mechanics*, Vol. 68, pp. 1371-1384, 2001.
[14] Cavallini, G., Galatolo, R., Cattaneo, G., An experimental and numerical analysis of multi-site damaged butt-joints, *Proceedings of the 20th ICAF Symposium*, Vol. 1, Bellevue, Washington, U.S.A., July 1999.
[15] Garcia, A. N., Irving, P. E., *A study of geometrical correction factors in a MSD scenario, Presented at the Civil Aviation Authority – U.K.*, Report no. CAA/W30637E/57, Cranfield University, Damage Tolerance Group, U.K., 2003.

Copyright Statement